JOURNAL OF CATALYSIS **167,** 447–459 (1997)
ARTICLE NO. CA971601

Effect of Metallo-organic Precursors on the Synthesis of Sm–Sn Pyrochlore Catalysts: Application to the Oxidative Coupling of Methane

A. C. Roger, C. Petit, and A. Kiennemann

LERCSI, URA CNRS 1498, ECPM, 1 rue Blaise Pascal, 67008 Strasbourg, France

Received April 26, 1996; revised October 25, 1996; accepted December 30, 1996

Synthesis of a series of $Sm_2Sn_2O_7$ pyrochlore catalysts by a sol-gel-like method has been developed. The preparation from the oxides gives stoichiometric pyrochlore, unlike the result obtained when starting from chlorinated salts ($SmCl_3$ or $SnCl_2$), which form tin-deficient pyrochlores. A spectroscopic study of the behaviour of the starting oxides or chlorides in propionic acid, to generate a series of precursors, has been carried out, particular attention being focused on the precursors generated by $SnCl_2$ in propionic acid using ^{119}Sn NMR and FTIR spectroscopy. The formation of $SnCl_2(C_2H_5COO)_2$ as the main precursor is responsible for the tin deficiency observed in the pyrochlore structure. The catalytic performance in oxidative coupling of methane is directly correlated with the tin deficiency in the bulk of the pyrochlore. The work highlights the importance of controlling precisely the synthesis of the catalysts.

INTRODUCTION

The catalytic conversion of methane into C_2 hydrocarbons by oxidative coupling (OCM) has given rise to an abundant literature during the past decade. Numerous works report systematic screening of active and selective catalysts. A review of some of the systems has been published by Maitra (1). This approach did not lead to catalytic systems likely to be efficient enough for industrial application on account of the limited experimental C_2 yield. Moreover, the formulation of the best catalysts was complex and the reproducibility difficulties exclude potential industrial development. Screening is now outmoded and a strategy for the development of more selective catalysts has been developed both in the field of chemical engineering (reactor design, optimization of the reaction conditions) (2) and at the catalytic system preparation level (3). An understanding of the oxidation reactions (production of CO_2 and CO/H_2) should also permit the enhancement of the selectivity to C_2 (3, 4).

It has been clearly established that the adsorption of oxygen on the catalytic surface leads to an equilibrium between various anionic oxygen species (5) and that this surface equilibrium is essential for the orientation of the reaction towards C_2-hydrocarbon formation or deep oxidation into CO_2. This surface phenomenon is directly affected by the bulk properties of the solid. In this view of how the bulk can influence the surface reactions, numerous studies have been carried out, for example, on specific surface area (6), morphology (7), crystalline structure (8), electrical conductivity (9–11), oxygen mobility (8), and carbonation (12).

Although the first step of the oxidative coupling of methane (abstraction of one H atom of CH_4) is typically a surface reaction, the coupling of two $CH_3\cdot$ radicals to form C_2H_6 and the dehydrogenation of ethane to C_2H_4 are thought to occur mainly in the gas phase *via* a radical mechanism (13). To elucidate this point, numerous studies on the effect of chlorinated gas addition were carried out (14–16). In this case chlorine acts under the form of $Cl\cdot$ in the gas phase and is able to propagate the radical reactions. Its beneficial effect on the C_2-selectivity is immediate and ends as soon as the chlorinated gas is removed from the reaction flow. With the aim of maintaining the chlorine effect over a period of time, catalytic systems were synthesized from chlorinated starting salts (17–21). In this case chlorine is thought to modify the surface properties of the catalyst. The presence of chlorine lowers the amount of highly basic sites (22, 23) and induces the creation of new active sites (18).

Particular structures can be prepared by different methods from various starting salts, in particular with chlorinated salts. They are well described in the literature and are easily characterizable. Perovskites (ABO_3) were the object of abundant works, especially barium-based ones (24, 25). Pyrochlores ($A_2B_2O_7$), known for their malleability and their ability to exist as a nonstoichiometric phase, were also studied. The attraction of the pyrochlore structure lies in its intrinsic anionic vacancies (26) (compared with the fluorite structure $A_2B_2O_8$) likely to favour oxygen adsorption. Ashcroft *et al.* (27) were among the first to study tin-based pyrochlores for catalytic behaviour. $Sm_2Sn_2O_7$ was presented as being mainly fully oxidizing (H_2O and CO_2 production). Our laboratory, on the other hand, published

0021-9517/97 $25.00

results for this pyrochlore (28) where a C_2-yield of 19.7% was obtained. These two $Sm_2Sn_2O_7$ systems were prepared from different starting salts and by two different methods but in both cases pyrochlore structures were obtained.

Preparation by firing–milling can lead to well-defined structures after high-temperature treatments. In this method the starting materials, generally oxides, carbonates, or nitrates, are ground together and pelletized before calcination. Alternative methods such as sol-gel or coprecipitation, owing to intimate mixing of the elements by formation of mixed precursors, permit the crystallisation of the same structures at lower calcination temperatures. These methods present the advantage of being valid for a large variety of starting salts (including chlorides) and solvents. Propionic acid reacts with numerous cationic starting salts to form propionates, so this solvent was often used for the sol-gel-like synthesis (named the "resin method") of particular structures (20, 24, 29), viz. perovskite, bixbyite, and pyrochlore. In the resin method, propionate precursors oligomerize in solution. However, unlike the real sol-gel synthesis, colloidal particles are not obtained.

The aim of the present work was to elucidate the role of the starting salts (oxides, chlorides) and that of propionic acid in the preparation by the resin method, of a series of Sm–Sn pyrochlores to understand why drastic differences in the catalytic behaviour were encountered in the literature (27, 28). The various steps of the synthesis were studied: the dissolution of the starting salts in propionic acid, the precursors which are thus generated, the behaviour of these precursors from the solution to the resin formation and the resin calcination which leads to the pyrochlore structure. The final purpose was to understand the links between preparation, structure, and catalytic behaviour of these pyrochlore catalysts in the methane oxidative coupling reaction.

EXPERIMENTAL

Pyrochlore Synthesis

The synthesis of the pyrochlores is based on the resin method (29) from metallo-organic propionate precursors. The metallic elements (Sm and Sn) were introduced into the oxide (Sm_2O_3: 99.9% purity, Strem; SnO: 99% purity, Strem) and chloride ($SmCl_3$: 99.9% purity, Strem; $SnCl_2$: anhydrous, 98% purity, Strem) forms by the preparation route summarized in Fig. 1.

First, samarium and tin salts were separately dissolved in an excess of hot propionic acid ($T \sim 120°C$). The concentration of all the solutions was 0.1 mol · liter^{-1}. The solutions were mixed and the excess of solvent was evaporated. A translucent resin was obtained, which was then heated to 750°C at 2°C min^{-1} and held at this temperature for 4 h to form the pyrochlore.

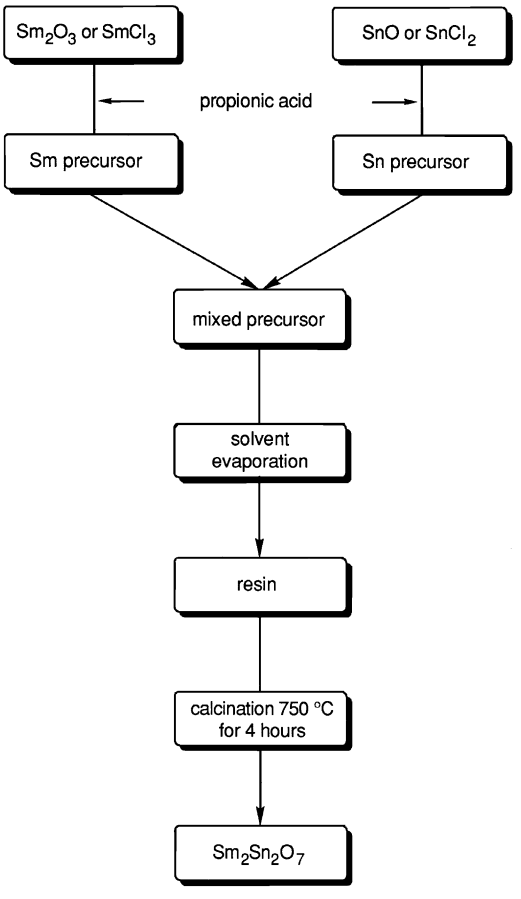

FIG. 1. Pyrochlore preparation scheme.

The mixing of propionic samarium solution from Sm_2O_3 with various proportions of propionic tin solutions from SnO and $SnCl_2$, as well as propionic tin solution from SnO with various starting proportions of propionic samarium solutions from Sm_2O_3 and $SmCl_3$, led us to prepare seven pyrochlores labelled A–G, the compositions of which are given later in Table 4 under Results and Discussion. A notation was adopted such that, for example, $[Sm_2O_3]$-2[SnO(75%)–$SnCl_2$(25%)] means that all the Sm atoms were introduced in the Sm_2O_3 form, that 75% of the tin atoms were in the SnO form and 25% in the $SnCl_2$ form, the Sm/Sn atomic ratio being equal to 1/1. It must be noted that samarium and tin were always introduced in order to have a Sm/Sn atomic ratio equal to 1/1, corresponding to the stoichiometric $Sm_2Sn_2O_7$ pyrochlore.

For comparison, Sm_2O_3 (cubic) was also prepared by the resin method using propionic acid.

Pyrochlore Characterization

X-ray diffraction. Pyrochlore catalysts were ground to a fine powder before being analyzed by X-ray diffraction. The XRD operating conditions were as follows: a Co tube

TABLE 1

Specific Surface Areas of Catalysts A to G

Catalyst	A	B	C	D	E	F	G
BET surface area before test ($m^2\ g^{-1}$)	8.2	26.9	32.7	21.2	17.3	12.1	20.0
BET surface area after test ($m^2\ g^{-1}$)	6.3	17.9	27.6	27.0	17.3	14.5	23.1

($K\alpha$ wavelength = 1.789 Å) at 40 kV and 25 mA, the angle scanned was from 25 to 100 2θ (step 0.05 2θ, time 1 s). The diffraction diagrams were compared to that of $Sm_2Sn_2O_7$ given in the JCPDS pattern number 21–1427. From the four most intense diffraction peaks (222, 400, 440, and 622) the cubic lattice parameter was calculated as follows: $a = d_{hkl}(h^2 + k^2 + l^2)^{1/2}$, and compared to the theoretical value of 10.51 Å.

Specific surface area measurements. The specific surface areas were measured by the BET method based on the N_2 physisorption capacity at 77 K.

The values obtained for the seven prepared pyrochlores before and after catalytic test are given in Table 1.

Elemental analysis. The weight percentages of Sm, Sn, and Cl were determined by atomic absorption in the "Service Central d'Analyse du CNRS," Vernaison. From these results the atomic ratios were calculated.

X-ray photoelectron spectroscopy. The analyses were performed on a VG ESCA 3 apparatus. The kinetic energy of the emitted photoelectrons (in eV) is given by: $E_{\text{kin.}} = 1486.6 - E_{B\text{cor.}}$, where 1486.6 eV is the energy of the incident radiation (Al$K\alpha$) and $E_{B\text{cor.}}$, the corrected binding energy of the electron. Binding energies were calibrated with respect to the signal for adventitious carbon (C_{1s} binding energy = 284.8 eV).

The corrected intensity of A (given element) is given by

$$I_{A\text{cor.}} = \frac{I_{A\text{meas.}}}{n_A \cdot \sigma_A \cdot \sqrt{E_{\text{kin.}A}}},$$

where I_A is measured intensity (experimental), n_A is the scan number (experimental), and σ_A is the cross-section (tabulated).

The ratio of the corrected intensities of two elements A and B directly accounts for the A/B atomic ratio at the surface of the analyzed sample.

Precursor Characterization

FTIR studies. The cationic precursors generated by the dissolution of Sm_2O_3, $SmCl_3$, SnO, and $SnCl_2$ in propionic acid were crystallized with hexane as countersolvent. To each solution, hexane was slowly added at ambient temperature until a cloudiness appeared. The solutions were then kept at −15°C for 2 days. The solid precursors were filtered out and washed with hexane.

In the case of the solution from $SnCl_2$, three distinct solids were successively obtained (products 1, 2, and 3 in the order in which they were obtained). It must be noted that the melting point of product 3 was so low that its filtration and its subsequent analysis by FTIR spectroscopy were made difficult. Other products of lower melting point are thought to remain in solution.

The same process can be carried out on the mixed Sm–Sn solutions to follow the evolution of the precursors after the mixing of the samarium and tin solutions. It was made in the case of the mixed solution generated by $SmCl_3$ and SnO (pyrochlore G, see Table 4 below).

The crystallized products were then analyzed by FTIR using a Nicolet 5DXC spectrometer with a scan number per spectrum of 50 for products 1 and 2, and 20 for product 3. For each analysis 3 mg of product were ground with 97 mg of KBr and then pelleted into a disc of 13 mm diameter.

^{119}Sn NMR studies. The ^{119}Sn nucleus has a spin +1/2, its natural abundance is 7.61% (30).

The performed experiments were one-pulse experiments in unlocked mode. The pulse width was 9 μs, the acquisition time was 0.294932 s, and the scan number was 1800.

The NMR analyses were carried out at 300 K in propionic acid as solvent, in a 10-mm liquid type probe. They were referenced to $Sn(Me)_4$ in C_6D_6 (2/98 vol) by the substitution method (external reference) and were performed on a Bruker AM 400 apparatus which gives for tin a frequency of 149.2 MHz.

The solution of $SnCl_2$ in propionic acid (0.15 mol · liter^{-1}) was studied. Then, 3, 6, 10, and 25% vol of H_2O were added to the initial solution.

Catalytic Tests

The catalytic tests were carried out in a U-shaped quartz reactor (i.d. = 6.6 mm). The reaction conditions were: total gas flow, 12 liters · h^{-1} · g cat^{-1}; CH_4/O_2/He mole ratio, 2/1/12; and the reaction was followed between 400 and 800°C. The reaction products were separated by gas chromatography on Hayesep D 3 m ∅ 1/8 in. and Carbosieve SII 1 m ∅ 1/8 in. columns and detected by TCD.

The definitions relative to the catalytic activity are

$$\text{Conversion of reactants } (CH_4 \text{ or } O_2)\ (\%) = 100 * \frac{\text{moles of transformed reactant}}{\text{moles of initial reactant}}$$

and

$$\text{Selectivity to products } (\%) = 100 * \frac{CH_4 \text{ moles transformed into the given product}}{\text{total transformed } CH_4 \text{ moles}}.$$

Here, products are CO, CO_2, C_2H_4 or C_2H_6; H_2O is also

produced but not quantified; traces of C_3 hydrocarbons are detected; and $S(C_{2+})$ is the sum of the selectivities to C_2H_4 and C_2H_6.

$$\text{Yield in given product (\%)} = \frac{\text{CH}_4 \text{ conversion (\%)} * \text{selectivity (\%) to product}}{100}.$$

RESULTS AND DISCUSSION

Precursor Characterization

Solid Samarium Precursors

Precursors generated by Sm_2O_3 in propionic acid solution. Samarium oxide reacts with propionic acid to form samarium propionates, characterized, in the solid state, by FT-IR (ν_{as} COO of 1564 and 1543 cm^{-1}, δ_{as} CH_3 at 1469 cm^{-1}, δ_s CH_3 at 1385 cm^{-1}) (Fig. 2a). Propionates are present in two forms stable in air: bidentate (1543 cm^{-1}) and monodentate (1564 cm^{-1}), as shown in Scheme 1.

Precursors generated by $SmCl_3$ in propionic acid solution. The infrared spectrum of the crystallized precursor (Fig. 2b) shows vibrations at 600 and 480 cm^{-1}. They can be assigned

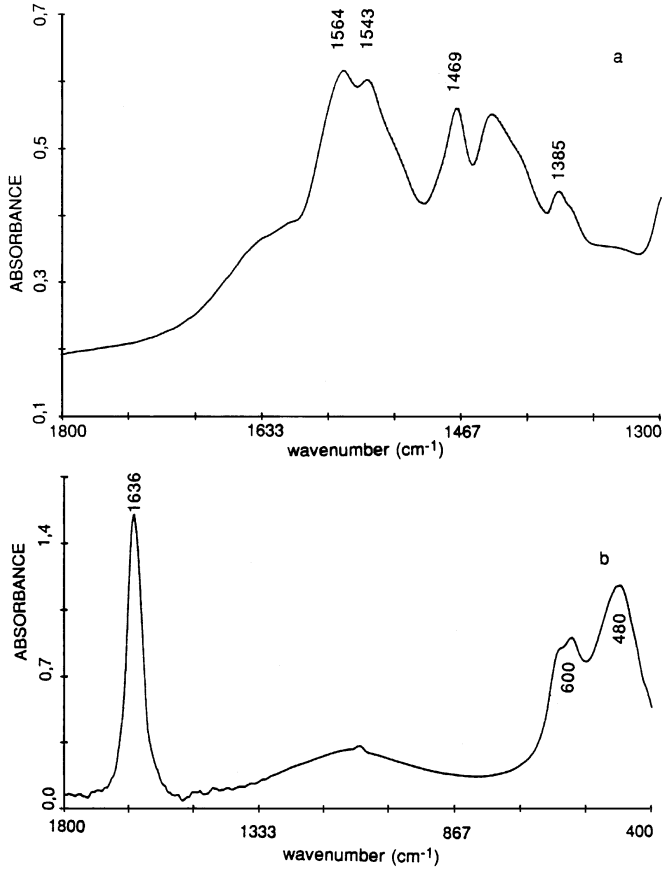

FIG. 2. IR spectra of Sm precursor solids generated by (a) Sm_2O_3 in propionic acid solution and (b) $SmCl_3$ in propionic acid solution.

bidentate Sm complex

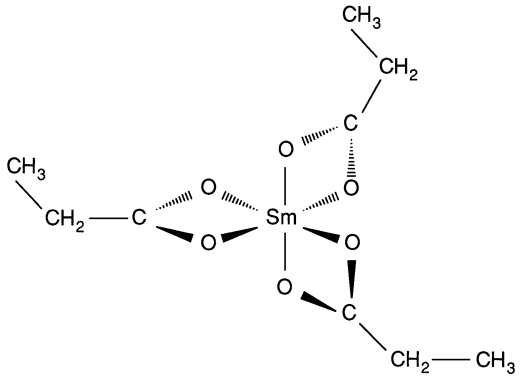

monodentate Sm complex

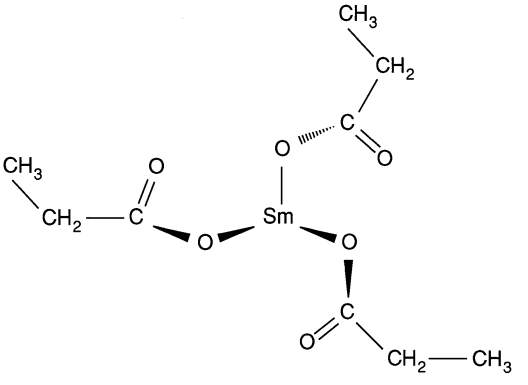

SCHEME 1

to Sm–Cl bonds. The band at 1636 cm^{-1} indicates that the product used is partially hydrated. Contrary to what occurs with Sm_2O_3, the dissolution of $SmCl_3$ in propionic acid does not result in propionate formation (which would be detected at 1564 and/or 1543 cm^{-1}, see Fig. 2, spectrum 2a), but is only a solvation phenomenon.

Tin Precursors

Precursors generated by SnO in propionic acid solution. The dissolution of SnO in propionic acid under argon is impossible. Oxygen supply in the solution makes this step easier.

The infrared spectrum of the crystallized compound (Fig. 3) exhibits characteristic bands of bidentate tin propionate (ν_{as} COO at 1528 cm^{-1} and ν_s COO at 1410 cm^{-1}) (11) and reveals the presence of a H_2O ligand (1623 cm^{-1}) (31). The presence of this H_2O band together with the beneficial effect of oxygen addition during dissolution can be interpreted by an oxidation of Sn(II) into Sn(IV) according to the following scheme:

$$\text{Sn(II)} + \tfrac{1}{2}\text{O}_2 + 2\text{H}^+ \rightleftharpoons \text{Sn(IV)} + \text{H}_2\text{O} \qquad [1]$$

standard potential: $\Delta E^\circ = 1.078$ V (32).

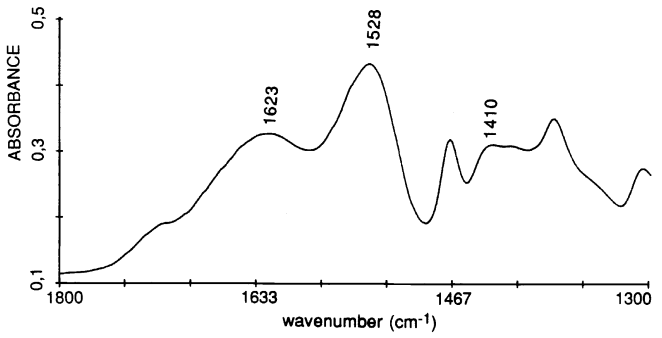

FIG. 3. IR spectrum of Sn precursor solid generated by SnO in propionic acid.

Taking into account the variation of oxidation number of tin from II to IV, the tin precursor from SnO can be written as $Sn(C_2H_5COO)_a\ (H_2O)_b$, where $0 \le a \le 4$, $0 \le b \le 4$, and $a + b = 4$.

Precursors generated by $SnCl_2$ in propionic acid solution: FTIR study of the solid precursors. By progressive addition of hexane to the solution of $SnCl_2$ in propionic acid (15 g in 200 ml), three distinct solids (1, 2, and 3) were obtained. Their infrared spectra between 1800 and 1300 cm^{-1} are presented in Fig. 4.

Product 1 presents ester-like (monodentate) propionate vibration bands (33) (ν_{as} COO at 1582 cm^{-1} and ν_s COO at 1399 cm^{-1}) and bridging (bidentate) propionate (ν_{as} COO at 1535 cm^{-1} and ν_s COO at 1410 cm^{-1}). In product 1, the monodentate form is predominant. The two forms coexist in product 2 (ν_{as} COO at 1577 cm^{-1} for the monodentate, ν_{as} COO at 1529 cm^{-1} for the bidentate propionate). Product 3 is only in the form of bidentate propionate (ν_{as} COO at 1526 cm^{-1}). In this last product a H_2O ligand is detected (1612 cm^{-1}) (31).

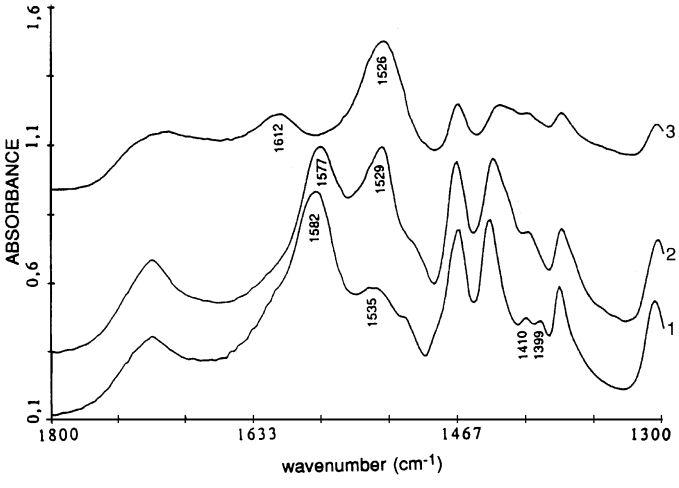

FIG. 4. IR spectra of precursors generated by $SnCl_2$ in propionic acid. (1) product 1; (2) product 2; (3) product 3.

The shift from 1535 cm^{-1} (product 1) to 1526 cm^{-1} (product 3) of the bidentate propionate ν_{as} COO vibration can be correlated with the presence of chlorine ligands on tin (11, 34): two chlorine ligands in product 1, one chlorine ligand in product 2, and product 3 would be free of chlorine.

Precursors generated by $SnCl_2$ in propionic acid solution: ^{119}Sn NMR study. Further information was obtained from ^{119}Sn NMR analysis of the solution of $SnCl_2$ in propionic acid (0.15 mol · liter^{-1}), the spectrum of which is given in Fig. 5a. According to Yeh and Geanangel (35), the chemical shift (δ) of the ^{119}Sn NMR signal of Sn (II) dissolved in a solvent of dielectric constant $\varepsilon < 7$ (ε for propionic acid = 3.3) should be in the range of 0 to −200 ppm (depending on the concentration). In our case the signals are in the range of δ between −600 and −680 ppm. As in the case of SnO, the dissolution of $SnCl_2$ in propionic acid implies oxidation of Sn(II) into Sn(IV), a reaction which occurs with H_2O formation (see Eq. [1] above).

Four NMR signals can be noted on this spectrum. The tin propionates are known to be monomeric in solution (35, 36), thus no Sn–Sn coupling is expected. The quadrupole moment of chlorine is high ($-0.079|e|10^{-24}$ cm^2) (37) and hides the Sn–Cl scalar coupling. Each NMR signal corresponds to only one chemical species. Thus the diversity of tin precursors evidenced by FTIR is confirmed, in solution, by ^{119}Sn NMR.

Taylor and Coddington (38) studied by ^{119}Sn NMR a series of complexes $[SnCl_{6-n}(H_2O)_n]^{n-2}$, where $0 \le n \le 6$. In our case, since there was evidence for propionate ligands by FTIR, the multiple signals as well as the tin oxidation (joined to water formation) are interpreted by the creation of a family of complexes of general formula: $[SnCl_x(C_2H_5COO)_{y/2}(H_2O)_z]^{4-x-y/2}$ with $x + y + z = 6$. These complexes would be expected to exhibit D_{4h} symmetry (39). The propionate ligands will be considered as bidentate. However, propionates are probably in the two forms (36). According to the work of Taylor and Coddington (38), in the family $[SnCl_{6-n}(H_2O)_n]^{n-2}$, δ increases with the number of Cl ligands on tin: from −620 ppm for $n = 5$ to −720 ppm for $n = 0$. By analogy, the signals at −663 and −628 ppm (see Fig. 5a) could be assigned to complexes where chlorine ligands are present ($x > 0$, in the former given family), and the two other signals to species free of chlorine ($x = 0$, $y + z = 6$). To assign more precisely the species, increasing amounts of water were added to the initial solution in order to modify the relative proportions of the complexes $[SnCl_x(C_2H_5COO)_{y/2}(H_2O)_z]^{4-x-y/2}$. When the charge $(4 - x - y/2)$ is different from zero, propionate or chloride ions can play the role of counterions. The ^{119}Sn NMR spectra of the solutions containing 3, 6, and 10% in volume of H_2O are presented in Figs. 5b–5d.

As soon as 3 vol% of H_2O is added to the initial solution, the two highest chemical shift peaks diseappear (spectrum 5b compared to 5a). These signals are attributed to

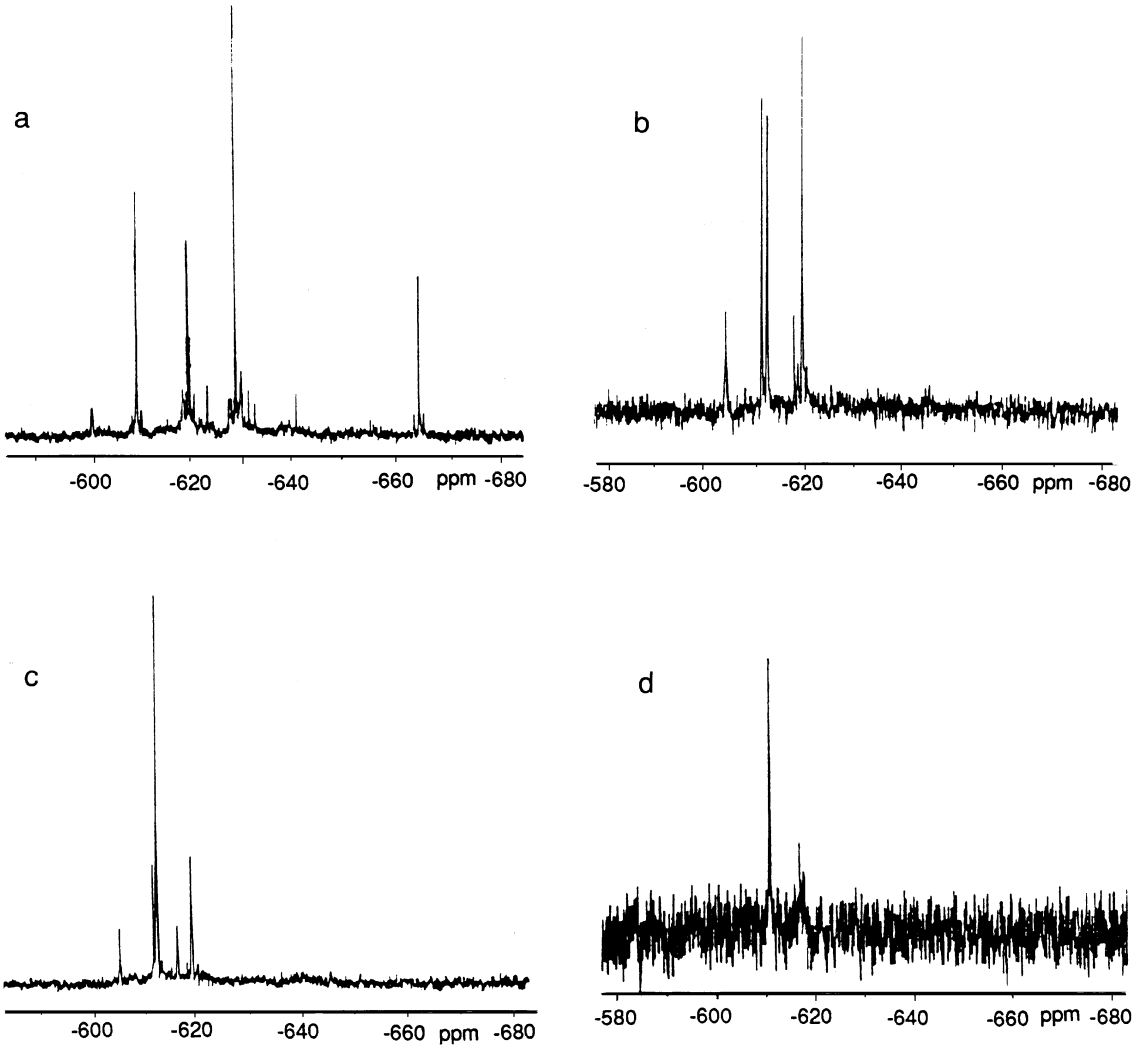

FIG. 5. ^{119}Sn NMR spectrum of $SnCl_2$ in propionic acid (a) without addition of H_2O; (b) + 3 vol% H_2O; (c) + 6 vol% H_2O; and (d) + 10 vol% H_2O.

chlorinated complexes such as those shown as I and II in Scheme 2. Complex I is neutral (Sn is IV). Complex II has a +1 charge and the released Cl^- remains in the first coordination sphere (38).

The signals not yet assigned vary between −619 and −601 ppm. The corresponding species are free of chlorine ($x = 0$) with increasing amounts of H_2O ligands. Their chemical shifts and intensities are summarized in Table 2.

The intensity of signals at −619 and −612 ppm decreases with increasing H_2O addition. The intensity of those at −618 and −601 (value which shifts to −603 and −605 ppm) remains almost constant. The intensity of the −613 ppm signal increases.

The various complexes which must be considered are:

- $x = 0$, $y = 4$, $z = 2$ (complexes III and IV, Scheme 3).
- $x = 0$, $y = 2$, $z = 4$ (complexes V and VI, Scheme 4).
- $x = 0$, $y = 0$, $z = 6$ (complex VII, Scheme 5).

Complexes IV and VI, in which the propionate ligands are monodentate, can be considered as being structural isomers of the complexes III and V, respectively. Indeed, in III and V the propionate ligands are bidentate and the two oxygen ions are located in the plan of the D_{4h} structure, but in the case of IV and VI the axial position of one oxygen is less favoured and the propionate ligand tends to be monodentate (the complexes remaining in D_{4h} symmetry). It is consistent with the fact that, in solution, propionates are in the two forms (36).

The sum of the intensities of complex III and complex IV (structural isomers) should decrease with water addition to the benefit of complex V and complex VI (structural isomers). These complexes (V and VI) should lead to complex VII with a further addition of water, the NMR response of which would be weak because of its tendency to polymerize (38). Note that for 10 vol% of H_2O (Fig. 5d) the signal/noise ratio is much weaker than for Figs. 5a–5c.

tin complex I

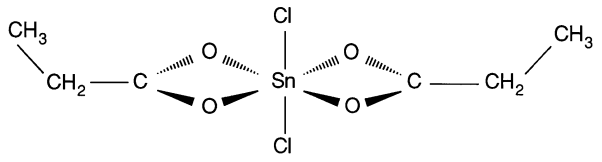

- 663 ppm
x=2 y=4 z=0

tin complex II

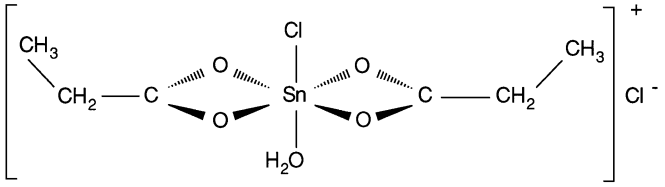

- 628 ppm
x=1 y=4 z=1

SCHEME 2

For 25 vol% of H_2O no signal was detected indicating that the defined geometry around the tin atom is lost, which is consistent with the formation of a hydroxide gel.

Table 2 and the preceding remarks led us to propose the following assignments of complexes:

- III or IV
  —stable signal at −619 ppm.
  —signal between −618 and −616 ppm. The intensity of this signal is always inferior to that at −619 ppm. One of the two isomers would be thermodynamically less favored and can thus be assigned to the less intense signal.

TABLE 2

Characteristics of the NMR Signals between −619 and −601 ppm

H_2O% in solution	−δ (ppm) intensity (%)				
0	619	618	—	609	601
	37	7	—	50	6
3	619	617	613	612	603
	32	8	25	26.5	8.5
6	619	616	613	612	605
	17	7.5	53	15	7.5
10	—	—	—	—	610
	—	—	—	—	—
Identification of complexes	III or IV		V or VI		VII

- V or VI
  —signal at −613 ppm. This peak appears from 3 vol% of H_2O. It probably comes from the −609 ppm peak splitting (−609 → −613 and −612 ppm with water addition). It largely predominant for 6% H_2O (53%).
  —signal at −612 ppm. For 3 vol% of H_2O, its intensity is comparable to that of the −613 ppm peak, then decreases with water addition. As for III and IV, V and VI are structural isomers. The more stable one would be assigned to the −613 ppm signal.
- VII
  —signal between −605 and −601 ppm.

Precursors generated by $SnCl_2$ in propionic acid solution: Links between FTIR and NMR studies. It is now possible to make a link between the infrared studies (on solid compounds) and the ^{119}Sn NMR experiments (in the liquid state). In both cases there is evidence for the oxidation of tin leading to the creation of a set of tin propionate precursors. The relative proportions of these precursors vary with the amount of water in the liquid medium. Addition of H_2O decreases the amount of chlorinated tin precursors.

Crystallized product 1 (2 Cl ligands on tin) can be correlated with complex I proposed from NMR studies: $SnCl_2(C_2H_5COO)_2$ corresponding to $x=2$, $y=4$, $z=0$ in the general formula $[SnCl_x(C_2H_5COO)_{y/2}(H_2O)_z]^{4-x-y/2}$.

tin complex III

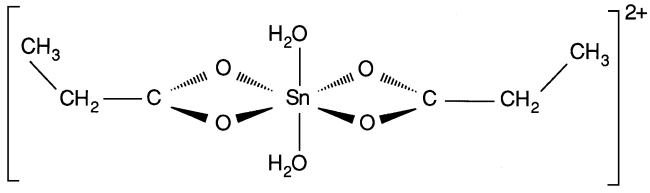

tin complex IV

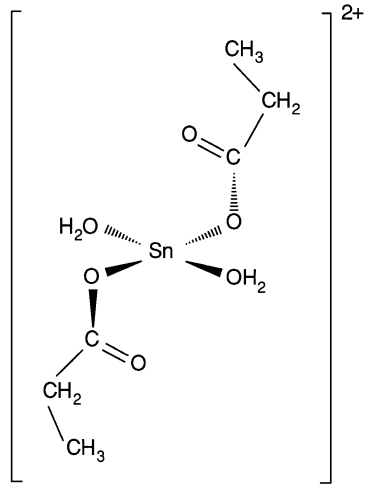

SCHEME 3

tin complex V

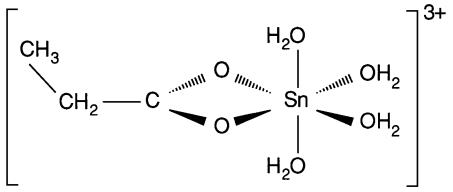

tin complex VI

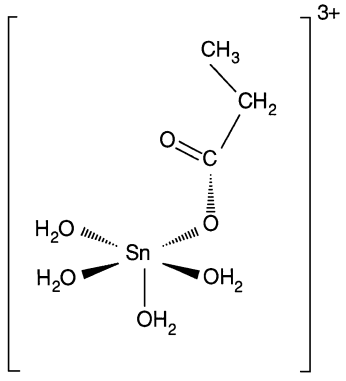

SCHEME 4

Product 2 and complex II can also be correlated, their formula being $[SnCl(C_2H_5COO)_2(H_2O)]^+$, corresponding to $x=1$, $y=4$, $z=1$ in the general formula given earlier. In this case, the H_2O ligand vibration should appear in IR, which is not the case. In the solid state, the tin carboxylates are known to polymerize (33, 36). A dimer form, coming from the condensation of two $[SnCl(C_2H_5COO)_2(H_2O)]^+$ monomers, with release of propionate and H_2O ligands, must be taken into consideration (Scheme 6).

Product 2 would then come from the dimerization of complex II. It is likely that, as for complex I, the propionate ligands of II in solution are monodentate and that the dimerization (or polymerization) due to the crystallization induces the bridging of these ligands.

tin complex VII

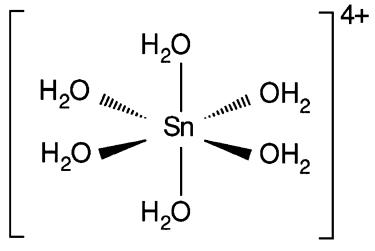

SCHEME 5

tin product 2

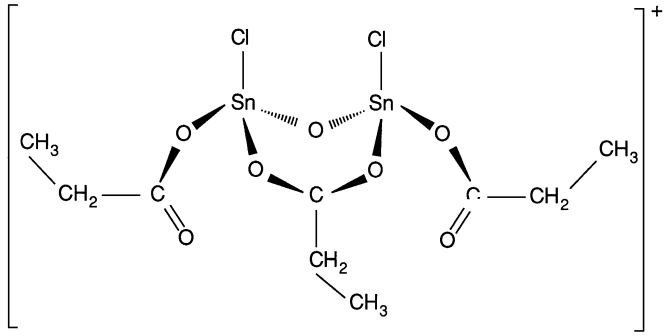

SCHEME 6

Product 3 is free of chlorine and could correspond to complexes III and IV. It is difficult to be sure whether the propionate ligands are bidentate or bridged between two tin atoms. Two formulations can be proposed (Scheme 7).

Complexes V, VI, and VII are only present in solution when H_2O is added. They do not correspond to any compound identified by infrared analyses because no water was added to the solution from which the solid tin precursors were prepared.

It must be noted that, among the mentioned tin precursors, product 1 (complex I) $SnCl_2(C_2H_5COO)_2$ is largely predominant. From gravimetric measurements it was shown that 58% of the tin dissolved in propionic acid from

monomeric tin product 3

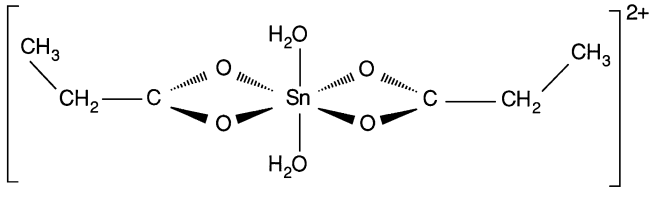

dimeric tin product 3

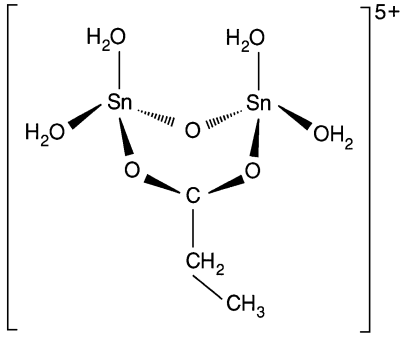

SCHEME 7

TABLE 3

Elemental Analysis of Product 1 Compared to $SnCl_2(C_2H_5COO)_2$

Weight %	C	H	O	Cl	Sn
Product 1	21.49	3.26	21.46	19.66	33.99
$SnCl_2(C_2H_5COO)_2$	21.47	3.01	19.07	21.12	35.35

$SnCl_2$ crystallizes as $SnCl_2(C_2H_5COO)_2$. The raw formula of this compound was confirmed by elemental analysis. The results are given in Table 3.

This part devoted to the characterization of the precursor (formed after reaction of the starting salts with propionic acid) can be summarized as follows:

Sm_2O_3 leads to $Sm(C_2H_5COO)_3$;

$SmCl_3$ leads to $SmCl_3$ solvated by propionic acid;

SnO leads to $[Sn(C_2H_5COO)_2(H_2O)_2]^{2+}$; and

$SnCl_2$ leads to the family

$[SnCl_x(C_2H_5COO)_{y/2}(H_2O)_z]^{4-x-y/2}$,

where $x + y + z = 6$.

The compound $SnCl_2(C_2H_5COO)_2$ is predominant when no H_2O is added to propionic acid. Addition of water to the solution of tin precursors from $SnCl_2$ induces the release of the Cl ligands and thus leads to the disappearance of the chlorinated precursors.

The mixing of the precursor solutions and the solvent evaporation will induce condensation reactions between the various precursors. The resin obtained is then heated to form the $Sm_2Sn_2O_7$ pyrochlore.

Pyrochlore Characterization

Characterization of the Catalytic Solids

The seven prepared pyrochlores A–G were characterized by XRD and elemental analysis. The results are summarized in Table 4. The XRD spectra of A and D are given in Figs. 6a and 6b.

For all the preparations, the diffraction analysis indicates the formation of only one cubic structure. Pyrochlore A exactly corresponds to $Sm_2Sn_2O_7$ synthesized by firing–milling (40). Its cubic lattice parameter (10.51 Å) is consistent with that given in the literature. The pyrochlores prepared from Sm_2O_3 and a mixture of SnO–$SnCl_2$ exhibit an enlarged lattice parameter (limiting value: 10.59 Å). Elemental analysis indicates that A is stoichiometric. However, increasing amounts of $SnCl_2$ to generate the tin precursors induce increasing Sm/Sn ratios in the pyrochlores, from Sm/Sn = 1.1 for B to Sm/Sn = 1.7 for D. It can really be said that the pyrochlores are substoichiometric in tin because in all cases (A to G) only one cubic structure was detected by XRD (see spectrum 6b). Despite the tin deficiency no Sm_2O_3 phase rejection occurs but pyrochlores crystallize with an enlarged lattice parameter. If present, Sm_2O_3 would be detected at $d = 3.16$ Å (main diffraction peak for cubic Sm_2O_3) which was never the case. The diffraction diagrams of A and D exhibit the diffraction peaks of the pyrochlore. No additional peak was detected. The only difference is the shift of d_{hkl} in the case of D. The diffraction peaks are shifted to higher angles and reflect the lattice enlargment.

After calcination at 750°C, pyrochlores E, F, and G are less crystallized than pyrochlores A to D. However, the trend shows that, as for B to D, the lattices are enlarged (10.54, 10.55, and 10.57 Å). The crystallization goes on during the catalytic tests which are carried out up to 800°C. After the test, the lattice parameter of pyrochlores E, F, and G is 10.59 Å. It must be noted that the use of $SmCl_3$ instead of Sm_2O_3 also induces increasing Sm/Sn ratios in the pyrochlores, from Sm/Sn = 1.1 for E to Sm/Sn = 1.7 for G.

The characterization of the pyrochlores points to a parallel behaviour between catalysts B, C, and D and catalysts E, F, and G with the variation of chlorinated starting salt. In both cases, chlorine coming from $SnCl_2$ (B, C, D) or from $SmCl_3$ (E, F, G), tin substoichiometric pyrochlore systems are obtained although they were prepared from stoichiometric mixtures of samarium and tin.

It must also be noted that substoichiometric tin pyrochlores are never obtained when a Sm_2O_3–SnO mixture (with initial tin deficiency) is used, contrary to what happens with Sm_2O_3–SnO–$SnCl_2$ (B, C, and D) and Sm_2O_3–$SmCl_3$–SnO (E, F, and G) mixtures. In that case pyrochlores crystallize only in the $Sm_2Sn_2O_7$ stoichiometric form ($a = 10.51$ Å) with Sm_2O_3 phase rejection.

TABLE 4

Characterization of the Pyrochlores

		XRD			
		Lattice parameter	Elemental analysis		
Name	Starting salts	a (Å)	Sm/Sn	Cl/Sm	Sn%
A	$[Sm_2O_3]$–2[SnO]	10.51	1.0	—	50
B	$[Sm_2O_3]$–2[SnO(90%)–$SnCl_2$(10%)]	10.54	1.1	0.1	45
C	$[Sm_2O_3]$–2[SnO(75%)–$SnCl_2$(25%)]	10.59	1.2	0.1	42
D	$[Sm_2O_3]$–2[$SnCl_2$]	10.59	1.7	0.4	29
E	[2$SmCl_3$(10%)–Sm_2O_3(90%)]–2[SnO]	10.54	1.0	0.0	45
F	[2$SmCl_3$(50%)–Sm_2O_3(50%)]–2[SnO]	10.55	1.3	0.2	38
G	[2$SmCl_3$]–2[SnO]	10.57	1.7	0.5	28

Note. XRD, elemental analysis, Sn% with respect to the total cationic amount.

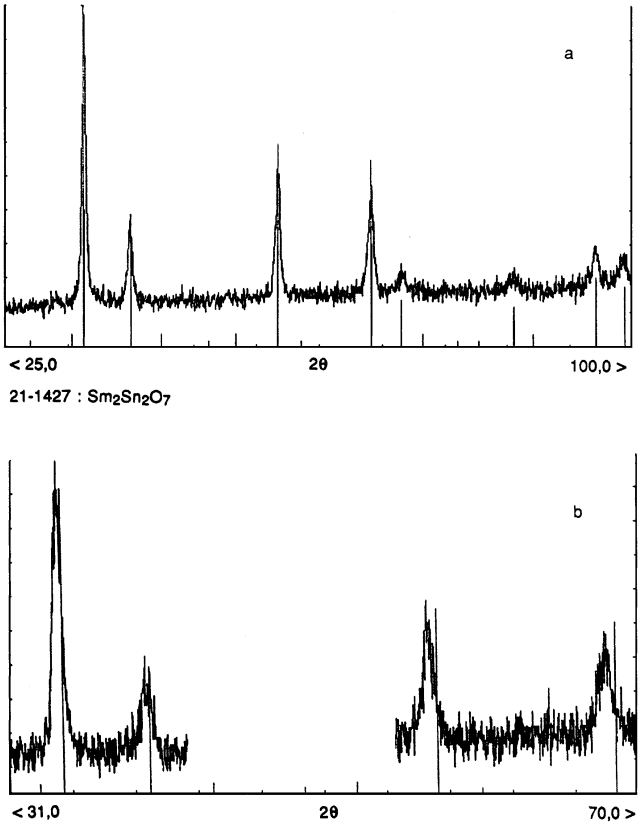

FIG. 6. X-ray diffractograms of (a) pyrochlore A, $[Sm_2O_3]$–2[SnO] and (b) pyrochlore D, $[Sm_2O_3]$–2$[SnCl_2]$.

Resin Characterization

A study of the resin obtained from Sm_2O_3–$SnCl_2$ (synthesis D) by thermogravimetric and differential thermal analysis (TGA-DTA) (Fig. 7) provides an explanation for the tin substoichiometry evidenced by elemental analysis (see Table 4).

Three distinct weight losses can be noted. The first weight loss corresponds to the evaporation of residual solvent (boiling point of propionic acid, 141°C) (endothermic reaction). The second zone, 150–330°C, corresponds to the pyrolysis of the ligands of the precursor (exothermic broad peak). In the third zone, the weight loss is sharp and occurs at 330°C. It was identified (by coupling TGA with mass spectral analysis) as the evaporation of the tin $SnCl_2(C_2H_5COO)_2$ metallo-organic compound (product 1 in IR, compound I in ^{119}Sn NMR) (endothermic reaction). This tin precursor does not react to form the pyrochlore, but leaves the resin at 330°C during the calcination step and induces a tin deficiency in the pyrochlore structure. This phenomenon was confirmed by the heating of product 1.

This evaporation explains why from A to D the tin deficit increases in the pyrochlores. The more $SnCl_2$ is added to SnO, the more $SnCl_2(C_2H_5COO)_2$ is formed and evaporates, inducing tin substoichiometry.

Table 4 indicated that the tin deficiency phenomenon was identical for pyrochlores B, C, and D (Sm_2O_3 and SnO–$SnCl_2$) and E, F, and G (Sm_2O_3–$SmCl_3$ and SnO). The propionic solution of SnO was shown to generate $[Sn(C_2H_5COO)_2(H_2O)_2]^{2+}$, whereas the solution of $SmCl_3$ was only its solvation by propionic acid. In order to understand the lack of tin in pyrochlores E, F, and G, the mixed solution of SnO and $SmCl_3$ was studied by FTIR after crystallization by hexane addition. The IR bands at 600 and 480 cm^{-1} (Sm–Cl vibrations) detected in Fig. 2b do not appear in the spectrum of the $SmCl_3$–SnO mixed precursor (not given). This indicates that samarium, initially solvated by propionic acid, in the form of $SmCl_3$, reacted. Propionate ligand vibrations are detected at 1534 cm^{-1} (ν_{as} COO), 1413 cm^{-1} (ν_s COO), 1467 cm^{-1} (δ_{as} CH_3), and at 1378 cm^{-1} (δ_s CH_3). Thus, ligand exchanges are proposed to occur. The Cl^- release from $SmCl_3$ when the tin precursor is added to the propionic solution of $SmCl_3$ permits to propose that, as for $SnCl_2$ in propionic acid, the precursor $SnCl_2(C_2H_5COO)_2$ is formed. This would explain why the pyrochlores B to D and E to G are comparable, because of the similarities of the phenomena which occur during the preparation. In both cases $SnCl_2(C_2H_5COO)_2$ would form in solution and would evaporate during the calcination to lead to tin substoichiometric pyrochlores.

It must be remembered that the amount of $SnCl_2(C_2H_5COO)_2$ in solution is strongly dependent on the amount of H_2O. Therefore, the problem of reproducing the results in these syntheses can be ascribed to the difficulty of controlling tin substoichiometry by controlling the water amount (20).

Crystalline Lattice Enlargement

The last point to explain is the enlargement of the lattice up to 10.59 Å. It can be correlated with the tin deficiency of the pyrochlore.

A representation of a quarter ($0 \leq z \leq 1/4$) of the unit cell of $Sm_2Sn_2O_7$ is given in Fig. 8. In order to represent an easily

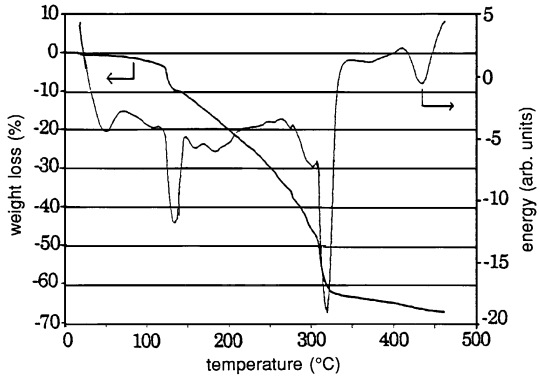

FIG. 7. Thermogravimetric analysis and differential thermal analysis of the resin $[Sm_2O_3]$–2$[SnCl_2]$ given D pyrochlore.

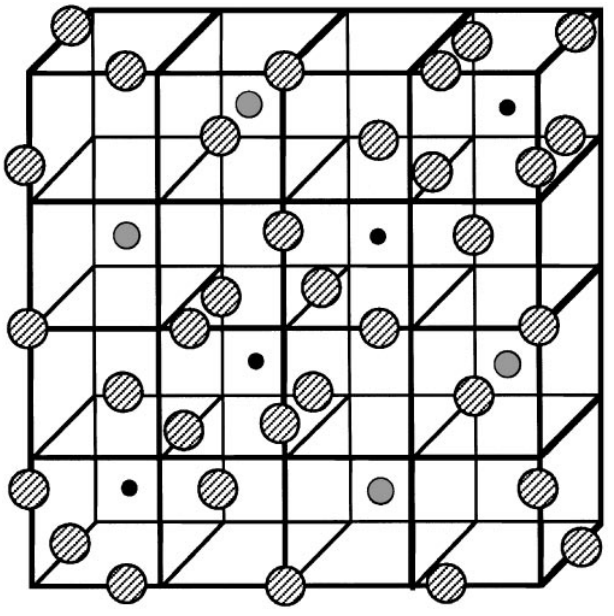

FIG. 8. Representation of one quarter of the $Sm_2Sn_2O_7$ lattice ($0 \le z \le 1/4$). ●, Sm (+III); •, Sn (+IV); ▨, O (−II).

understandable lattice, the crystallographic positions have been shifted according to ($x + 1/8$; $y + 1/8$; $z + 1/8$) so that the anions are located on the crystallographic axes.

Both tin deficiency of the pyrochlore and conservation of electroneutrality in the crystal cause a lack of SnO_2 groups in the structure. The local effect of SnO_2 deficiency is schematized in Fig. 9. The oxygen anions which surround the SnO_2 vacancy will tend to repel one another electrostatically and will prefer to adopt more favourable crystallographic positions.

Everything happens as if the ionic radius of the B cation were increased. The result is an enlargement of the lattice as in the $A_2B_2O_7$ pyrochlore families where A is a given cation and B represents cations with increasing ionic radii. For example (26), the lattice parameter of $Gd_2Ti_2O_7$ is 10.18 Å [$r(Ti^{4+}) = 0.605$ Å], that of $Gd_2Os_2O_7$ is 10.27 Å [$r(Os^{4+}) = 0.63$ Å], and that of $Gd_2Zr_2O_7$ equals 10.53 Å [$r(Zr^{4+}) = 0.72$ Å]. The ionic radius of Zr^{4+} is the highest a Sm-based pyrochlore can tolerate. Beyond this value the formation condition ($1.46 < r(A^{3+})/r(B^{4+}) < 1.80$) is no more fulfilled and the compounds will not crystallize in the pyrochlore structure. That explains why the increase of the lattice parameter of tin-deficient Sm–Sn pyrochlores is limited to 10.59 Å, value which is almost that of $Sm_2Zr_2O_7$ pyrochlore ($a = 10.594$ Å) (41).

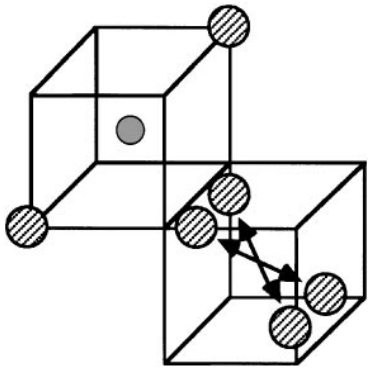

FIG. 9. Local effect of SnO_2 vacancy. ●, Sm (+III); ▨, O (−II).

Catalytic Tests

The seven prepared catalytic systems were tested for their reactivity in the oxidative coupling of methane and their ability to produce C_2-hydrocarbons (C_2H_4 and C_2H_6). They were compared to cubic Sm_2O_3, whose activity is higher than that of the monoclinic form (8). The pyrochlores A to G are ordered with increasing tin amounts (see Table 4) and their reactivities are given in Fig. 10.

Pyrochlore A (from Sm_2O_3 and SnO) is a strong oxidizing agent as indicated by Ashcroft *et al.* (27) and produces CO_2 and H_2O only. For pyrochlores B to D and E to G, methane conversion, C_2-selectivity, and C_2-yield increase linearly with decreasing amount of tin in the catalyst. At comparable amounts of tin (29 and 28%), pyrochlores D and G exhibit the same catalytic behaviour:

pyrochlore D: CH_4 conv. = 27.3%
C_2-sel. = 10.2%
C_2-yield = 2.8%
pyrochlore G: CH_4 conv. = 27.5%
C_2-sel. = 9.5%
C_2-yield = 2.6%

The most active catalyst is cubic Sm_2O_3. The higher the tin deficiency in the pyrochlore, the more the methane

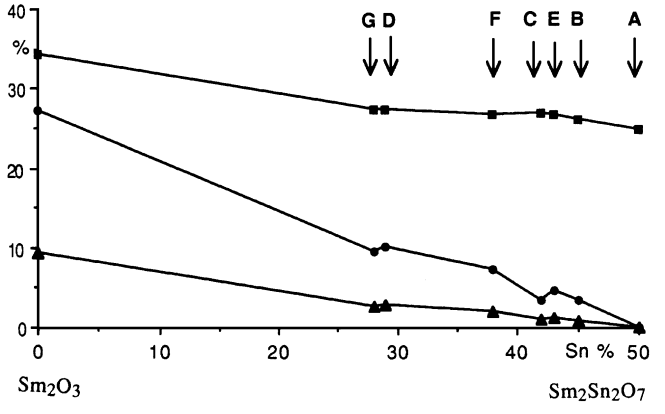

FIG. 10. Catalytic results for pyrochlores A to G and cubic Sm_2O_3. $CH_4/O_2/He = 2/1/12$ mole ratio; total gas flow, 12 liters $\cdot h^{-1} \cdot g\ cat^{-1}$; reaction temperature, $T = 775°C$. ■, CH_4 conversion; ●, C_2-selectivity; ▲, C_2-yield.

TABLE 5

Surface Sm/Sn and Cl/Sm Atomic Ratios of A, C, and H by XPS Analysis

Pyrochlore	A before test	A after test	C before test	C after test	H before test	H after test
Sm/Sn	0.51	0.33	0.75	0.46	0.45	0.36
Cl/Sm	—	—	0.51	0.17	0.27	0.13

oxidative coupling activity tends towards that of cubic Sm_2O_3 (CH_4 conversion, 34.3%; C_2-selectivity, 27.2%; and C_2-yield, 9.4% under our experimental reaction conditions).

The specific surface areas of the seven catalysts given under Experimental do not account for the evolution of the catalytic activity.

Elemental analysis showed that no chlorine was retained in the bulk after the catalytic tests, the Cl/Sm ratio being equal to zero in all cases.

The surface of three pyrochlores was examined by XPS: these were A, C, and the equivalent of C prepared from $SmCl_3$ (the pyrochlore [2$SmCl_3$(25%)–Sm_2O_3(75%)]–2[SnO], which will be designated H). It must be noted that the catalytic properties of H are consistent with the curves of Fig. 10 since CH_4 conversion, C_2-selectivity, and C_2-yield of H locate between those of E ($SmCl_3$(10%)) and F ($SmCl_3$(50%)). The peaks of Sn $3d_{5/2}$ (at 485.6 eV) and Sm $3d_{5/2}$ (at 1081.2 eV) indicate the unique formation of oxidation state of Sn^{4+} and Sm^{3+}. These data agree with the NMR studies and the formation of the pyrochlore structure. The surface Sm/Sn and Cl/Sm atomic ratios of A, C, and H before and after reactivity test are given in Table 5.

Note that an excess of tin was detected on the surface of the three systems. The phenomenon increases during the catalytic test. However, the variation of the Sm/Sn ratio is not linear since the values for A and H are comparable (0.51 compared to 0.45 and 0.33 compared to 0.36), while those obtained for C are always higher (0.75 and 0.46). Thus the reactivity behaviour is not related to the tin distribution on the surface.

Although no chlorine was detected in the bulk (elemental analysis), the XPS analyses of C and H reveal that even after the test a low amount of chlorine is retained at the surface (Cl/Sm = 0.17 for C and 0.13 for H). It must be added that, in the steady state, the catalytic results remain stable over 30 h and an effect of Cl · radicals in the gas phase can therefore be excluded.

The beneficial effect of chlorine in the reaction of oxidative coupling of methane due to the incorporation of chlorinated mineral compounds during the preparation of the catalysts (creation of new active sites, less highly basic sites) (22, 23) must be taken into consideration. However, as shown by elemental analysis, a small amount of chlorine is retained in the bulk after the calcination to form the pyrochlore. For all the pyrochlores, the (Cl/Sm) atomic ratio is equal to 0.0 after the reactivity test as indicated by elemental analysis, even for D and F (pyrochlores prepared from the most important amount of chlorinated starting salts) which presented before test the Cl/Sm atomic ratios, respectively, of 0.4 and 0.5. Despite the presence of some chlorine on the surface (shown by XPS), it can be said that the pyrochlore catalysts studied do not possess a high ability to retain chlorine introduced during the preparation step.

A structural effect has then to be considered to explain the catalytic results. As indicated in Fig. 10, the reactivity behaviour of catalysts A (C_2-yield, 0) to G (C_2-selectivity, 9.5%; and C_2-yield, 2.6%) tends, for increasing tin deficiency, to that of cubic Sm_2O_3 (lattice parameter of 10.93 Å) (C_2-selectivity, 27.2%; and C_2-yield, 9.4%). This result is consistent with the fact that with increasing tin deficiency the lattice parameter of pyrochlores B to D and E to F increases from 10.51 to 10.59 Å (for C and D) or 10.57 Å (for G).

The sol-gel synthesis via chlorinated starting salts is efficient for the enhancement of the reactivity of $Sm_2Sn_2O_7$ pyrochlores. However, the C_2 increase is not due to a pure "chlorine effect" as described in the literature. In our case the role of chlorine lies in the preparation step where $SnCl_2(C_2H_5COO)_2$ is formed. This precursor evaporates at 330°C during the calcination and induces tin deficiency in the structure. The greater the tin deficiency, the more the activity of Sm–Sn pyrochlore catalysts tends to that of cubic Sm_2O_3.

CONCLUSION

The knowledge of Sm–Sn pyrochlore synthesis acquired by studying the cationic precursors by FTIR and ^{119}Sn NMR has permitted mastery and control of the structure of the systems.

The formation of the tin precursor $SnCl_2(C_2H_5COO)_2$ which evaporates during the calcination step induces the crystallization of tin-deficient pyrochlores. The tin substoichiometry can be controlled either by the SnO–$SnCl_2$ relative proportions or by the water content of the liquid medium. These tin substoichiometric structures crystallize with an enlarged lattice parameter without any phase rejection.

The catalytic performances can be directly correlated with the tin deficiency and are similar when the catalysts are prepared from Sm_2O_3–$SnCl_2$ or from $SmCl_3$–SnO. This phenomenon was explained by the chlorine ligand migration from Sm to Sn in solution so that in both cases the same precursors are generated.

Since the phenomenon of the tin deficiency is mastered, it now becomes possible to take advantage of the bulk vacancies by doping such defective structures by elements

which are able to retain chlorine and known to be active in OCM. Indeed, if such elements are added to the solutions which contain Cl^- anions, they would be able to prevent chlorine from being released during the resin formation, then during the calcination step by stabilization in the defective structure. In addition to the beneficial effect of the tin deficiency, a C_2-selectivity enhancement due to a chlorine effect may occur. This part is developed in another work (42) where a stable C_2 yield of 20% has been obtained over more than 300 h.

REFERENCES

1. Maitra, A.M., *Appl. Catal.* **104**, 11 (1993).
2. Mleczko, L., and Baerns, M., *Fuel Process. Tech.* **42**, 217 (1995).
3. Martin, G. A., and Mirodatos, C., *Fuel Process. Technol.* **42**, 179 (1995).
4. Maitra, A. M., and Tyler, R. J., "Natural Gas Conversion II" (H. E. Curry-Hyde and R. F. Howe, Eds.), p. 265 (1994).
5. Zhang, Z., Verykios, X. E., and Baerns, M., *Catal. Rev. Sci. Eng.* **36**, 507 (1991).
6. Martin, G. A., and Mirodatos, C., "Methane Conversion by Oxidative Processes" (E. E. Wolf, Ed.), p. 351. Van Nostrand–Reinhold, New York, 1992.
7. LeVan, T., Che, M., Kermarec, M., Louis, C., and Tatibouët, J. M., *Catal. Lett.* **6**, 395 (1990).
8. Peil, K. Marcellin, G., Goodwin, J. G., and Kiennemann, A., "Novel Methods of Producing Olefins and Aromatics Chemical Series" (L. Albright and B. L. Crynes, Eds.), p. 61. Dekker, New York, 1991.
9. Dubois, J. L., and Cameron, C. J., *Appl. Catal.* **67**, 49 (1990).
10. Norby, T., and Andersen, A. G., *Appl. Catal.* **71**, 89 (1991).
11. Zhang, Z. L., and Baerns, M., *J. Catal.* **135**, 317 (1992).
12. Tang, C., Zang, J., and Lin, L., *Appl. Catal. A* **115**, 243 (1994).
13. Marquaire, P. M., Gueritey, N., Côme, G. M., and Baronnet, F., *Stud. Surf. Sci. Catal.* **81**, 149 (1994).
14. Burch, R., Squire, G. D., and Tsang, S. L., *Appl. Catal.* **46**, 69 (1989).
15. Ahmed, S., and Moffat, J. B., *Appl. Catal.* **58**, 83 (1990).
16. Ahmed, S., and Moffat, J. B., *J. Catal.* **121**, 408 (1990).
17. Burch, R., Chalker, S., Loader, P., Mariscal, R., Rice, D. A., and Webb, G., *Catal. Today* **13**, 301 (1992).
18. Warren, B. K., *Catal. Today* **13**, 311 (1992).
19. Zhou, X., Zhang, W., Wan, H., and Tsai, K., *Catal. Lett.* **21**, 113 (1993).
20. Roger, A. C., Petit, C., Hilaire, L., Rehspringer, J. L., and Kiennemann, A., *Catal. Today* **21**, 341 (1994).
21. Yoon, K. J., and Seo, S. W., *Appl. Catal. B Environ.* **7**, 237 (1996).
22. Hinson, P. G., Clearfield, A., and Lunsford, J. H., *J. Chem. Soc. Chem. Commun.* 1430 (1991).
23. Conway, S. J., and Lunsford, J. H., *J. Catal.* **131**, 513 (1991).
24. Teymouri, M., Petit, C., Bagherzadeh, E., and Kiennemann, A., *Catal. Today* **21**, 377 (1994).
25. Dissanayake, D., Kharas, K. C. C., Lunsford, J. H., and Rosynek, M. P., *J. Catal.* **139**, 652 (1993).
26. Subramanian, M. A., Aravamudan, G., and Subba Rao, G. V., *Prog. Solid. State Chem.* **15**, 56 (1983).
27. Ashcroft, A. T., Cheetham, A. K., Green, M. L. H., Grey, C. P., and Vernon, P. D. F., *J. Chem. Soc. Chem. Commun.* 1667 (1989).
28. Petit, C., Kaddouri, A., Libs, S., Kiennemann, A., Rehspringer, J. L., and Poix, P., *J. Catal.* **140**, 328 (1993).
29. Rehspringer, J. L., and Bernier, J. C., *Mat. Res. Soc. Symp. Proc.* **72**, 67 (1986).
30. Sanders, J. K. M., and Hunter, B. K., "Modern NMR Spectroscopy," 2nd ed. Oxford Univ. Press, New York, 1993.
31. Pitchon, V., Primet, M., and Praliaud, H., *Appl. Catal.* **62**, 317 (1990).
32. Weast, R. C., "Handbook of Chemistry and Physics," 64th ed., p. D156. CRC Press, Boca Raton, Florida, 1984.
33. Roy, A., *Inorg. Chim. Acta* **28**, L123 (1978).
34. Cummins, R. A., *Aust. J. Chem.* **17**, 594 (1964).
35. Yeh, H. O. M., and Geanangel, R. A., *Inorg. Chim. Acta* **52**, 113 (1981).
36. Henderson, A., and Holliday, A. K., *J. Organometal. Chem.* **4**, 377 (1965).
37. Brevard, C., and Granger, P., "Handbook of High Resolution Multinuclear NMR," p. 106. Wiley–Interscience, New York, 1981.
38. Taylor, M. J., and Coddington, J. M., *Polyhedron* **11**, 1531 (1992).
39. Mao, X. A., You, X. Z., and Dai, A. B., *Inorg. Chim. Acta* **156**, 177 (1989).
40. *Natl. Bur. Stand. (U.S.) Monogr.* **25**, 877 (1970).
41. Klee, W. E., and Weitz, G., *J. Inorg. Nucl. Chem.* **31**, 2367 (1969).
42. Roger, A. C., Petit, C., and Kiennemann, A., *Stud. Surf. Sci. Catal.* **101B**, 1273 (1996).